1

Diurnal, weekly, seasonal and spatial variabilities in carbon dioxide flux in different urban landscapes in Sakai, Japan

Masahito UEYAMA[1] and Tomoya ANDO[1]

[1]Graduate School of Life and Environmental Sciences, Osaka Prefecture University, 1-1, Gakuen-cho,

Naka-ku, Sakai, Osaka, 599-8531, Japan

Corresponding author: M. Ueyama, Graduate School of Life and Environmental Sciences,

Osaka Prefecture University, Sakai, Japan (miyabi-flux@muh.biglobe.ne.jp)

2

Abstract

To evaluate CO_2 emissions in urban areas and their temporal and spatial variability, continuous measurements of CO_2 fluxes were conducted using the eddy covariance method at three locations in Sakai, Osaka, Japan. Based on the flux footprint at the measurement sites, CO_2 fluxes from the three sites were partitioned into five datasets representing a dense urban center, a moderately urban area, a suburb, an urban park, and a rural area. A distinct biological uptake of CO_2 was observed in the suburb, urban park, and rural areas in the daytime, whereas high emissions were observed in the dense and moderate urban areas in the daytime. Weekday CO_2 emissions in the dense urban center and suburban area were approximately 50% greater than emissions during weekends and holidays, but the other landscapes did not exhibit a clear weekly cycle. Seasonal variations in the urban park, rural area, and suburban area were influenced by photosynthetic uptake, exhibiting the lowest daily emissions or even uptake during the summer months. In contrast, the dense and moderately urban areas emitted CO_2 in all seasons. CO_2 emissions in the urban areas were high in the winter and summer months, and they significantly increased with the increase in air temperature in the summer and the decrease in air temperature in the winter. Irrespective of the land cover type, all urban landscapes measured in this study acted as net annual CO_2 sources, with emissions ranging from 0.5 to 4.9 kg C m^{-2} yr^{-1}. The magnitude of the annual CO_2 emissions was negatively correlated with the green fraction; areas with a smaller green fraction had higher annual CO_2 emissions. Upscaled flux estimates based on the green fraction indicated that the emissions for the entire city were 3.3 kg C m^{-2} yr^{-1}, which is equivalent to 0.5 Tg C yr^{-1} or 1.8 Mt CO_2 yr^{-1}, based on the area of the city (149.81 km^2). A network of eddy covariance measurements is useful for characterizing the spatial and temporal variations in net CO_2 fluxes from urban areas. Multiple methods would be required to evaluate the rationale behind the fluxes and overcome the limitations in the future.

1. Introduction

Cities emit a considerable amount of carbon dioxide (CO_2) that is associated with human activities into the atmosphere (Canadell et al., 2007). Urban areas account for only a small percentage of the earth's land surface but emit 30–50% of total anthropogenic CO_2 (Mills, 2007; Stterthwaite, 2008), and thus, cities are important sources of the global CO_2 emissions. The CO_2 emissions among global cities are highly heterogeneous (Mills, 2007; Nordbo et al., 2012), and the temporal variability is high (Velasco and Roth, 2010). To evaluate the spatio-temporal variabilities in CO_2 emissions for global cities, studies using multiple methods, such as measurements (Velasco and Roth, 2010) and emission inventories (Oda and Maksyutov, 2011), are currently conducted.

Global CO_2 emissions have often been estimated using emission inventories based on point source databases, statistics for national and regional CO_2 emissions, and satellite remote sensing (Oda and Maksyutov, 2011). The major challenge for estimating global CO_2 emissions is to understand the spatio-temporal dynamics of CO_2 emissions in various cities. Because emissions data are used in top-down estimates of the global CO_2 budget (Peters et al., 2007; Schmel et al., 2001), a better estimate of CO_2 emissions from cities will improve our understanding of the global carbon cycle, including terrestrial and ocean fluxes.

To evaluate CO_2 emissions in cities and their temporal and spatial variabilities, continuous measurements of CO_2 fluxes have been conducted using the eddy covariance method in various urban landscapes, including dense urban built-up areas (Gioli et al., 2012; Grimmond et al., 2002, 2004; Kotthaus and Grimmond, 2012; Nimitz et al., 2002; Pawlak et al., 2011; Velasco et al., 2005), suburban areas (Bergeron and Strachan, 2011; Coutts et al., 2007; Crawford et al., 2011; Hirano et al., 2015; Moriwaki et al., 2006; Ward et al., 2013), urban parks (Kordowski and Kuttler, 2010), and urban forests (Awal et al., 2010), in several cities. These results have indicated that cities emits a considerable amount of CO_2 into the atmosphere from human activities, such as vehicle traffic and household heating in the wintertime. Even in urban parks, CO_2 was emitted to the atmosphere due to human activities (Kordowski and Kuttler, 2010). The magnitude of CO_2 emissions and its temporal variability depended on the city, associated with the type

of human activities under different climate conditions (Järvi et al., 2012; Moriwaki et al., 2006; Velasco et al., 2016; Ward et al., 2013, 2015), and the role of urban vegetation (Awal et al., 2010; Kordowski and Kuttler, 2010; Peters and McFadeen, 2012; Ward et al., 2015), showing considerable heterogeneities.

Multi-site eddy covariance towers were used to synthesize the data and showed that green fraction was the index that explained the spatial variability in annual CO_2 emissions (Nordbo et al., 2012; Velasco and Roth, 2010; Ward et al., 2015), because the green fraction has many possible factors that determine CO_2 emissions: a greater green fraction correlates to lesser road and population densities (Nordbo et al., 2012). Upscaling using the green fraction can provide a high-resolution map of direct CO_2 emissions from cities. Previous studies have examined the relationship between annual CO_2 emissions and the green fraction at a global scale (Nordbo et al., 2012; Velasco and Roth, 2010; Ward et al., 2015). It is unclear whether upscaling CO_2 emissions is possible within a city, because multi-site eddy covariance measurements within a city are often unavailable.

In this study, we present diurnal, weekly, seasonal, and spatial variabilities in the CO_2 fluxes continuously measured at three different locations within 5 km of each other in Sakai, Osaka, Japan. Considering flux footprint, the data represent five urban landscapes, including a dense urban center, a moderately urban area, a suburb, a rural area, and an urban park. Regardless of the landscape type, all landscapes emitted considerable CO_2 annually with different temporal metabolisms, providing a useful overview of anthropogenic CO_2 emissions.

2. Materials and methods

2-1. Study sites

Sakai is the second largest city in Osaka Prefecture, located in western Japan. The population was approximately 842,000 in 2015. Because the city is located on the eastern shore of Osaka Bay, sea breeze circulation is evident throughout the year, except when seasonal winds are not strong. The area is on a uniformly flat plane; the north-south and the east-west slopes are 0.0030° and 0.0024°, respectively. The climate of Sakai is temperate; the mean annual air temperature is 15.9°C, the maximum monthly mean air

103 temperature was 28.0°C in August, the minimum monthly mean air temperature was

104 5.2°C in January, and the mean annual precipitation was 1187 mm yr^{-1} between 1981 and

105 2010 according to the Japanese Meteorological Agency.

106 The Sakai city center (SAC) site (Fig. 1; Table 1) is located on a tower at the top of a

107 city office building (34°34′25″N, 135°28′59″E). The population density around the city

108 center is approximately 12150 km^{-2}, based on the Japanese Government Statistics. The

109 area is a densely built-up urban area with a mean building height of 10.7 ± 3.1 m. Because

110 the distributions of building heights were highly skewed toward low-height buildings, the

111 mean building height greater than 20 m was 36 m, which occupied 33% of the total

112 building area. Many arterial roads and two highways with heavy traffic are present within

113 the flux footprint. Because industrial and commercial areas are located in the western and

114 northern parts of the city, those areas are expected to show higher rates of human activity

115 than locations where residential areas are dominant.

116 The Oizumi Ryokuchi urban park (IZM) site (Fig. 1; Table 1) is located at the northern

117 end of the city (34°33′48″N, 135°32′1″E), and was established in 1972. The

118 measurements were conducted at a tower located at the eastern edge of the park. Because

119 of the consistent presence of a sea breeze, the tower is mostly located downwind of the

120 park during the daytime. The land cover of the park consists of 51% trees, 15% grassland,

121 and 34% other, such as ponds, buildings, pavement, and bare ground. No vehicle traffic

122 was allowed in the park except parking. Measurements using a plant canopy analyzer

123 (LAI-2000, LI-COR, Lincoln, Nebraska, USA) showed that the leaf area index of trees

124 ranged from 3.2 to 5.7 m^2 m^{-2} with a mean of 4.3 m^2 m^{-2} in the summer months. The mean

125 and maximum tree heights were estimated as 12.3 ± 4.1 m and 21 m, respectively, using

126 a digital surface model by Google Earth. The area surrounding the IZM is a mixed

127 landscape of residential areas and agricultural fields and is characterized as a rural area

128 (Table 1). The population density of surrounding residences surrounding the IZM is

129 approximately 7940 km^{-2}, based on the Japanese Government Statistics.

130 The Osaka Prefecture University (OPU) site (Fig. 1; Table 1) is located at the western

131 edge of Osaka Prefecture University (34°32′50″N, 135°30′10″E). Because the

132 measurements were conducted on the roof of a building, the flux footprint represents only

133   a small suburban area. The western part of the site contains a protected forest on a kofun

134   (the ancient burial mound), Mozu Kofungun. The area is characterized as a suburb,

135   consisting of a university, a residential area, small streets, a graveyard, and trees. The

136   mean and maximum tree heights were 13.1 ± 2.9 m and 19 m, respectively, and the mean

137   and maximum building heights are 9.1 ± 2.9 m and 15 m, respectively.

138

139   *2-2. Observations*

140   We measured CO_2 fluxes using the eddy covariance method at the three sites. For SAC,

141   a sonic anemometer (SAT550, Sonic Corp., Tokyo, Japan) and an open-path infrared gas

142   analyzer (LI-7500, LI-COR) were installed on a 16-m tower located at the top of the city

143   office building (111 m above the ground) at the end of November, 2009. For IZM, a sonic

144   anemometer (CSAT3, Campbell Scientific Inc., Logan, Utah, USA) and an open-path

145   infrared gas analyzer (EC150, Campbell Scientific Inc.) were installed 30 m above the

146   ground on a tower at the end of January 2015. For OPU, sonic anemometers and several

147   infrared gas analyzers were installed on a 2-m mast above the rooftop at the edge of the

148   building (16.2 m above the ground) in November 2014. Turbulent fluctuations were

149   recorded at 10Hz using a datalogger (8421, Hioki, Japan) for SAC and dataloggers

150   (CR1000, Campbell Scientific Inc.) for IZM and OPU.

151   For the OPU site, eddy covariance systems were periodically changed. A sonic

152   anemometer (DA600, Sonic Corp.) was in place from November 2014 to March 2015 and

153   again in November 2015. A different sonic anemometer (Model 81000, R. M. Young,

154   Traverse, Michigan, USA) was in place from March 2015 to April 2015, and a third type

155   of sonic anemometer (Windmaster, Gill Instruments, Lymington, UK) was in place in

156   April 2015. The eddy covariance system was initially a closed-path system using a gas

157   analyzer (LI-6262, LI-COR), until March 2015, and was then changed to an open path

158   system using an open-path infrared gas analyzer (LI-7500, LI-COR). Another eddy

159   covariance system using a sonic anemometer (DA600, Sonic Corp.) and an open-path

160   infrared gas analyzer (LI-7500, LI-COR) was installed on a different edge of the building

161   in November 2015. This additional measurement system increased data acquisition,

162   because we eliminated the data coming from the roof. Consequently, CO_2 fluxes were

calculated based on the different systems with relevant corrections. We confirmed that there was no significant difference between open-path and closed-path systems through an inter-comparison (RMSE = 2.18 μmol m^{-2} s^{-1}; F_{open} = 1.00 * F_{closed} - 0.03 μmol m^{-2} s^{-1}; R^2 = 0.84; F_{open} and F_{closed} represent CO_2 fluxes by the open and closed paths, respectively), but these flux measurements have higher uncertainties than those from the other sites.

Meteorological and environmental variables were measured at each site. The air temperature, relative humidity, and incoming solar radiation were measured at the three sites. Rainfall, atmospheric pressure, incoming longwave radiation, and ground heat fluxes at the top of the building were measured at OPU. The leaf area index was manually measured approximately once a month using a plant canopy analyzer (LAI-2000, LI-COR) at ten forested sectors in IZM.

The gas analyzers were periodically calibrated. Because the open-path gas analyzer for SAC was installed at a location to which gas cylinders could not be carried easily, we calibrated the analyzer by comparing the signals of CO_2 and H_2O densities from a closed-path analyzer (LI-840, LI-COR), whose inlet was located near the open path analyzer. The closed-path analyzer was calibrated every four months using a known CO_2 gas, zero CO_2 gas and a dew point generator (LI-610, LI-COR). For OPU, the gas analyzers were calibrated at three times in 2015 using the gases and the dew point generator. For IZM, maintenance was regulated, and thus the analyzer was only calibrated at the start and end of the measurements.

2-3. Data analysis

In this study, we used one-year eddy covariance data measured in 2015 at SAC and OPU and the period from February 2015 to January 2016 at IZM. Turbulent fluxes were calculated with the eddy covariance method using the Flux Calculator program (Ueyama et al., 2012). Before the half-hourly covariance of vertical wind velocity and scalar quantities were calculated, spike data were removed from the raw data. No trend removal was applied. The artificial fluctuations of sonic air temperature associated with water vapor were corrected. The vertical wind velocity was coordinated as the mean vertical

193   wind velocity was equal to zero using the double rotation method. The angle-of-attack

194   errors for the Gill Instruments and R. M. Young anemometers were corrected based on

195   Nakai and Shimoyama (2012) and Kochendorfer et al. (2012), respectively. The high-

196   frequency loss for line averaging and sensor separation was corrected using theoretical

197   transfer functions for the open-path systems (Massman, 2000) and empirical transfer

198   functions for the closed-path system (Moore, 1986). Air density fluctuations were

199   corrected based on Webb et al. (1980).

200   Filtering of the nighttime data using the friction velocity (u_*) threshold was not applied

201   in this study. This was because (1) no clear threshold was obtained in nighttime data, (2)

202   data coverage at night was small due to the limited flux footprint, and (3) sensible heat

203   fluxes in the summer months often showed positive values even at night, except for IZM.

204   Our handling of nighttime data was the same as in previous studies in urban areas (e.g.,

205   Liu et al., 2012), but a potential underestimate of nighttime fluxes may have occurred.

206   The storage term was added to the turbulent fluxes for the vegetative site (IZM), whereas

207   storage was not considered for urban sites (SAC and OPU). The storage term for IZM

208   was estimated based on CO_2 concentrations at the height of the eddy covariance

209   measurements.

210   Flux data were selected for each landscape after a quality test and footprint analysis.

211   First, we applied the quality test to remove half-hourly flux data that included noise based

212   on a criterion (Appendix B.1 in Ueyama et al., 2012). A stationary test, an integral

213   turbulence test, and a higher moment test were applied, because flow statistics did not

214   strongly differ with ideal surfaces (Kaimal and Finnigan, 1994); σ_w/u_* at neutral

215   conditions were 1.3 for SAC, 1.5 for OPU, and 1.3 for IZM; σ_u/u_* at neutral conditions

216   were 2.6 for SAC, 2.6 for OPU, and 3.2 for IZM, where σ_w and σ_u are the standard

217   deviation of vertical and horizontal wind velocities, respectively. Half-hourly data were

218   subdivided into 5 minutes, and then the covariance was calculated for the 5-minute data.

219   If the difference between the mean of the covariance for the subdivided classes and half-

220   hourly covariance was greater than 40% of the half-hourly covariance, the data was

221   rejected as instationary (Foken and Wichura, 1996). We rejected the data when the

222   turbulent intensity was greater than 50% for IZM and 200% for SAC and OPU of the

intensities predicted by the similarity theory. According to the high moment test (Vickers and Mahrt, 1997), we removed data when the absolute value of skewness was greater than 3.6 or when the value of kurtosis was greater than 14.4. The fluxes, measured when winds came from the tower directions, were also removed. For OPU, the fluxes, measured when winds came from the directions of the building, were also removed. For SAC, based on a footprint model (Kormann and Meixner, 2000), we rejected data, when the source area contributing 80% of the flux footprint contained sea and mountains. Similarly, for IZM, we rejected flux data, when the source area contributing 50% of the flux footprint exceeded the boundary of the urban park. The displacement height was estimated based on MacDonald et al. (1998) for SAC, whereas those for the other sites were estimated at 0.7 times of the mean building or tree heights.

Depending on the wind direction, flux data at IZM and SAC were divided into two data series. For IZA, the flux data from the west represented the urban park, whereas data from other directions represented the rural area consisting of mixed residential and agricultural areas (Fig. 1). For SAC, flux data from the west represented the densely built-up urban center, whereas data from other directions represented the moderate urban to residential area (Fig. 1). Here, we defined the moderate urban area having a green fraction of 27%, which was double that of the dense urban built-up area (Table 1). Consequently, we formed five flux datasets from measurements at the three sites in 2015 for SAC and OPU and in the period from February 2015 to January 2016 in IZM: a dense urban center (west SAC), a moderately urban area (east SAC), a suburb (OPU), an urban park (west IZM), and a rural area (east IZM). Data coverage was 11% in west SAC, 21% in east SAC, 31% in OPU, 16% in west IZM, and 13% in west IZM.

Partitioning CO_2 fluxes into gross photosynthetic and respiratory fluxes was conducted only for the west and east IZM and OPU datasets, because the apparent daytime uptake was measured. The flux partitioning was conducted using the Flux Analysis Tool program (Ueyama et al., 2012). First, the relationship between nighttime CO_2 fluxes and air temperature was established based on a model (Lloyd and Taylor, 1994). The relationship was determined daily with a 49-day moving window. The gross photosynthetic flux was calculated as the difference between the estimated respiratory flux and the measured CO_2

253   flux. Because the estimated respiratory fluxes consisted of biological fluxes and nighttime

254   anthropogenic fluxes, it is important to note that the estimated gross photosynthetic fluxes

255   did not truly represent gross primary productivity, which is often used in ecosystem

256   studies (e.g., Baldocchi, 2008).

257   Gaps in the five datasets were filled using the Flux Analysis Tool program. First, small

258   data gaps for periods of less than 2.0 h were filled by linear interpolation. Second, for the

259   west and east IZM datasets, gaps were filled using a combination of a look-up-table and

260   non-linear regression methods (Ueyama et al., 2012), an approach well established for

261   use in natural ecosystems (Ueyama et al., 2013). For data gaps from the west and east

262   SAC and OPU, mean diurnal variations were applied, in which a mean diurnal pattern

263   was created daily using a 51-day moving window. Two mean diurnal patterns were

264   created, one for weekdays and one for weekends and holidays according to the weekly

265   cycle.

266   For evaluating vegetation activity in response to solar radiation (R_s), CO_2 fluxes (F_c)

267   for IZM and OPU were regressed for summer months using the following rectangular

268   hyperbola

269

270      $$F_c = -\frac{P_{max}\, b R_s}{P_{max} + b R_s} + R_d \qquad\qquad (1)$$

271

272   where P_{max} is the maximum photosynthetic rate, b is the initial slope, and R_d is dark

273   respiration.

274

275   *2-4. Upscaling using GIS data*

276   The annual CO_2 flux was upscaled according to the relationship between annual fluxes

277   and the green fraction. The green fraction was estimated using green census data

278   developed by the government of Sakai City. The green census data were created using

279   high-resolution aerial photographs from August 2001, which consisted of polygons of an

280   approximately 5-m spatial resolution. Based on the high-resolution polygon data, the

281   green fraction was evaluated at a 500-m spatial resolution. Because the green census data

often classified water as green area, we masked the water area using a land cover data

based on a geographical information system (Digital Map 5000 for the Kinki region in

2008 by the Geospatial Information Authority of Japan).

3. Results

3-1. Meteorological characteristics

The air temperature and vapor pressure deficit (VPD) showed clear seasonal variations (Fig. 2). The air temperature was lowest in January (5.9°C) and highest in August (28.2°C), based on a meteorological station of the Japanese Meteorological Agency. From late July to mid-August, the daily maximum air temperature was continuously higher than 30°C (Fig. 2a). Even in the winter, the daily minimum air temperature often did not reach negative values. The daytime maximum VPD was high from late April to mid-October, but showed a decline in a rainy season, called Baiu, from late June to mid-July, and the typhoon season starting from early September (Fig. 2b). The annual rainfall was 1324 mm yr^{-1} in 2015.

Due to a sea breeze, each site had distinct wind characteristics (Fig. 3). In SAC, winds mainly came from the northwest and east sectors. Winds came from the west and northwest sectors in OPU, and the winds came from the west to north sectors and an east sector in IZM. These characteristics were consistent throughout the seasons (Fig. A1).

3-2. Diurnal variations

Diurnal variations at SAC showed greater CO_2 emissions during the daytime than at night ($p < 0.01$) (Fig. 4). Daytime emissions were greater in the dense urban center (west SAC) than in the moderately urban area (east SAC) throughout the seasons ($p < 0.01$). Emissions from the urban areas were significantly higher in the daytime than in the nighttime in all seasons ($p \leq 0.01$). Such diurnal variations were similar to those for traffic counts measured by highway exits within the flux footprint (Fig. 4b). Note that the traffic counts at the exits peaked in the evening, whereas those at the entries could peaked in the morning (data not shown). Based on a comparison for diurnal cycles under different weather conditions, CO_2 emissions in the afternoon tended to be higher on sunny days

312   than on rainy or cloudy days for both the west ($p < 0.01$) and east ($p = 0.33$) SAC (Fig.

313   A2a, b). In contrast to CO_2 fluxes, there was no significant difference in the traffic counts

314   for sunny and rainy/cloudy days.

315   In contrast to SAC, CO_2 fluxes in OPU and IZM showed distinct daytime uptake

316   especially in summer months (Fig. 4). The magnitude of the daytime uptake was stronger

317   in the urban park than in the rural area. A daytime uptake was also observed at OPU in

318   the summer months from April to August. For these three landscapes, the CO_2 uptake

319   increased with solar radiation. According to the rectangular hyperbola regressed between

320   CO_2 fluxes and solar radiation, the rural area (R^2=0.46) and urban park (R^2=0.34) of IZM

321   have a stronger light-dependency than the suburb in OPU (R^2=0.10). The high light-

322   dependency in the urban park and the rural area suggests that light was the major

323   controlling factor in CO_2 fluxes at the diurnal timescale. This was consistent with the

324   smaller CO_2 uptake on rainy or cloudy days than on sunny days in the rural area (Fig.

325   A2e). For the urban park and OPU, the lack of a significant difference among weather

326   conditions (Fig. A2c, d) suggests that CO_2 fluxes were also influenced by other factors,

327   such as spatial heterogeneity and temperature conditions. For example, sunny days were

328   warmer in the daytime (approximately 2.5°C in the afternoon) and colder (approximately

329   1.1°C just before the sunrise) in the nighttime than rainy/cloudy days.

330

331   *3-3. Seasonal variations*

332   Different urban landscapes showed different seasonal variations in the CO_2 flux (Fig.

333   6). Similar to the diurnal variations, distinct biological signals were observed at IZM in

334   the urban park and rural area. The daily mean CO_2 fluxes showed lower emissions with

335   occasional negative values during summer months in both IZM sites. The suburban site

336   of OPU generally showed CO_2 emissions throughout the seasons, but the emissions rate

337   tended to be lower in the spring than in other months. The SAC site showed high CO_2

338   emissions throughout the seasons, and higher emissions were observed in the dense urban

339   center than in the moderately urban area. The seasonal variations in SAC exhibited two

340   distinct peaks during the summer and winter periods.

341   The seasonal variations in the daily CO_2 flux were dependent on the daily mean air

342 temperature and exhibited different patterns in different landscapes (Fig. 7). For the urban

343 site of SAC, CO_2 emissions increased as temperatures decreased (0.46-0.27 g C m^{-2} d^{-1}

344 ^{1} °C $^{-1}$; $p < 0.1$) when the mean daily temperature was less than 10°C. Higher CO_2

345 emissions were also observed at higher temperatures in SAC. An increase in CO_2

346 emissions at higher temperatures tended to also be observed at OPU ($p = 0.26$). Gas

347 consumption by university buildings within a footprint of OPU was consistent with the

348 two seasonal peaks revealing higher consumption in the summer and winter months (Fig.

349 A3). In the urban park and rural area, CO_2 emissions decreased as temperatures increased

350 above 15°C: -0.27 g C m^{-2} d^{-1} °C $^{-1}$ for the urban park ($p < 0.01$) and -0.13 g C m^{-2} d^{-1} °C

351 $^{-1}$ for the rural area ($p < 0.01$) when the mean air temperatures were greater than 15°C

352 (Fig. 7).

353 Gross photosynthetic fluxes were greater in the summer months than in the winter

354 months (Fig. 6). Surprisingly, the gross photosynthetic fluxes in the urban park and OPU

355 were comparable, probably due to the contributions of trees around the university and

356 from the kofun at OPU. The gross photosynthetic fluxes for the rural area were

357 approximately half of those for the urban park and OPU. The gross photosynthetic fluxes

358 for the three sites increased as temperatures increased to more than 20°C at 0.15-0.38 g

359 C m^{-2} d^{-1} °C $^{-1}$ ($p < 0.01$).

360

361 *3-4. Weekly variations*

362 Among the five landscapes, distinct weekly cycles of CO_2 emissions were only

363 observed at the west SAC and OPU sites (Fig. 8). On average, CO_2 emissions on

364 weekdays were approximately 50% greater than emissions on weekends and holidays (p

365 < 0.01) at the west SAC and OPU sites, even though the weekday CO_2 flux at the east

366 SAC was 10% higher than the fluxes on holidays ($p < 0.01$). The greater emissions on

367 weekdays were consistently observed throughout all seasons, and were consistent with

368 the traffic counts from the highway exits, where traffic was approximately 23% higher on

369 weekdays than on weekends and holidays (Fig. 4b).

370

371 *3-5. Annual CO_2 balance and its spatial variations*

372   All urban landscapes measured in this study acted as net source of CO_2 emissions on
373   an annual timescale (Fig. 9; Table 2). The strength of the annual CO_2 emissions was
374   negatively correlated with the green fraction ($R^2 = 0.96$; $p < 0.01$); areas with a smaller
375   green fraction had higher annual CO_2 emissions. The annual CO_2 emissions estimated in
376   this study were lower than those examined using a global synthesis by Nordbo et al.
377   (2012) (Fig. 9).
378   Based on the significant relationship between the green fraction and the annual CO_2
379   flux, the annual CO_2 fluxes were upscaled to the city scale (Fig. 10). Because the green
380   fraction of Sakai was low in the north and high in the south (Fig. 10a), annual CO_2
381   emissions were greater in the north than the south (Fig. 10b). The annual CO_2 fluxes from
382   the entire city were 3.3 kg C m^{-2} yr^{-1}, which corresponds 0.5 Tg C yr^{-1} or 1.8 Mt CO_2 yr^{-1}
383   based on the area of the city (149.81 km^2). The estimated emissions were lower than an
384   inventory-based estimate published by the government from 2000 to 2012 (8.0 ± 0.6 Mt
385   CO_2 yr^{-1}).
386
387   **4. Discussion**
388   Annual CO_2 emissions from Sakai City were in the range of those measured in other
389   studies, but tended to be at the lower end of the range (Fig. 9). For the same fraction of
390   green area (in this case, the green fraction was less than 20%), urban emissions ranged
391   from 4 to 18 kg C m^{-2} yr^{-1} for other cities (Nordbo et al., 2012; Velasco and Roth, 2010).
392   CO_2 emission in our city was lower than those measured in urban centers: a dense urban
393   built-up area in London (12.7 kg C m^{-2} yr^{-1}; Ward et al., 2015), the historical city center
394   in Florence (8.3 kg C m^{-2} yr^{-1}; Gioli et al., 2012), and a residential area of south central
395   Vancouver (6.7 kg C m^{-2} yr^{-1}; Christen et al., 2012). The annual emissions in our city
396   were also lower than previous cities that had a similar population density; there were only
397   two cities whose populations were higher than that in our city, but the annual emissions
398   in our city were seventh in the global synthesis (Fig. 12b in Ward et al., 2015). The low
399   CO_2 emissions rate in Sakai City was evident in the daytime peaks during the winter
400   months (Fig. 4), compared with a dense urban built-up area in London (e.g., more than
401   50 μmol m^{-2} s^{-1}, Ward et al., 2015) and a low built-up area in Beijing (30 μmol m^{-2} s^{-1},

402   Liu et al., 2012). Warmer winter temperatures (Fig. 2a) may contribute to lower emissions

403   as a result of reduced building heating and thus lower annual emissions in Sakai City

404   compared with other northern cities. The annual emissions rate in our urban center was

405   comparable to those of the densely populated residential areas in Yoyogi, Tokyo (4.3 kg

406   C m^{-2} yr^{-1}, Hirano et al., 2015), and Kugahara, Tokyo (3.4 kg C m^{-2} yr^{-1}, Moriwaki and

407   Kanda, 2004).

408   The sensitivity of the CO_2 emissions to cold temperatures was comparable to that

409   described in the previous studies (Bergeron and Strachan, 2011; Liu et al., 2012; Pawlak

410   et al., 2011). The effect of building heating has often been estimated as a slope between

411   air temperature and the CO_2 emissions rate: -2.02 g C m^{-2} d^{-1} $°C^{-1}$ in London (Ward et al.,

412   2015), -0.21 g C m^{-2} d^{-1} $°C^{-1}$ in Łódź (Pawlak et al., 2011), and -0.35 g C m^{-2} d^{-1} $°C^{-1}$ in

413   Beijing (Liu et al., 2012). These values are comparable to those obtained in our city: -

414   0.37 g C m^{-2} d^{-1} $°C^{-1}$ for all SAC ($p = 0.03$) and -0.27 g C m^{-2} d^{-1} $°C^{-1}$ for east SAC ($p <$

415   0.01), when mean air temperatures were less than 15°C (Fig. 7), although the correlation

416   for west SAC was insignificant. No sensitivities to cold temperatures were found in the

417   urban park (west IZM), rural area (east IZM), or residential area (OPU), which could be

418   due to the mixed effects of biological and anthropogenic signals.

419   CO_2 emissions in urban landscapes (SAC and OPU) also increased as temperatures

420   increased in the summer months (Fig. 7): 0.22 g C m^{-2} d^{-1} $°C^{-1}$ in west SAC ($p = 0.01$),

421   0.24 g C m^{-2} d^{-1} $°C^{-1}$ in east SAC ($p = 0.02$), and 0.13 g C m^{-2} d^{-1} $°C^{-1}$ in OPU ($p = 0.26$).

422   The high daytime CO_2 emissions were also examined on sunny days when the daytime

423   air temperature was higher than rainy/cloudy days (Fig. A2). Since traffic did not show a

424   clear seasonal variation (Fig. 4b), the reason for this increase is unclear, but one

425   possibility is the contribution of emissions from gas-powered air conditioners (Fig. A3).

426   The prevalence rate of gas- powered air conditioners is approximately 20% in non-

427   residential buildings, based on an assessment by the Japan Gas Association. The water

428   vapor flux in the summer months also significantly increased above a mean daily air

429   temperature of 17°C (T. Ando, unpublished data), suggesting gas consumption by air

430   conditioners. Kanda et al. (1997) also measured the high water vapor flux in the summer

431   at an urban center, Tokyo, and suggested that gas consumption associated with cooling

towers was responsible. In contrast to residences, tall buildings often use gas-based air conditioners, including the Sakai city office and buildings at OPU; especially after the Fukushima nuclear disaster at 2011, nuclear power plants that service the study area do not operate. Consequently, gas-based air conditioners increased (Agency for Natural Resources and Energy, 2015). A weaker dependence in OPU probably occurred because emissions from gas-powered air conditioners from the university building (Fig. A3) were negated by an increase in biological uptake (Fig. 6b). The sensitivity of gross photosynthetic fluxes to warming temperatures was 0.38 g C m^{-2} d^{-1} °C^{-1} in OPU ($p <$ 0.01).

Weekly cycles of CO_2 emissions were only observed at urban sites (Fig. 8), representing the strength of human activities. Previous urban CO_2 flux studies reported that major contributors to anthropogenic emissions were vehicle emissions and gas consumption (Gioli et al., 2012; Hirano et al., 2015; Velasco et al., 2005; Ward et al., 2013). Velasco and Roth (2010) indicated that weekly cycles were primarily related to vehicle emissions. The traffic count was high on weekdays at SAC (Fig. 4b), and business offices including the university are often more active on weekdays than on weekends and holidays. In contrast, there was no clear weekly cycle in the urban park, and the rural area. Large differences between weekdays and holidays in west SAC and OPU suggest greater contributions of emissions from vehicles and business offices compared with other landscapes. This underscores the importance of temporal variations in CO_2 emissions by land use.

The urban park acted as a net annual CO_2 source despite the abundant vegetation. Several factors explain the annual emissions from the urban park. First, the urban park frequently suffered from various management activities, such as harvesting and weeding. Such frequent disturbances could decrease the sink and increase source (Gough et al., 2007; Latty et al., 2004). A warmer climate in the urban area may induce higher respiration (Awal et al., 2010). A limited footprint might influence CO_2 fluxes arising from emissions from surrounding areas. We re-checked the data selection using stricter criteria according to which we rejected data when 80% of the flux footprint exceeded the boundary of the urban park, but the results were almost the same. Annual CO_2 emissions

462 of $2.4 \text{ kg C m}^{-2} \text{ yr}^{-1}$ were previously measured at an urban park in Germany (Kordowski
463 and Kuttler, 2010).

464   Partitioning the flux data measured at a single site with distinct landscapes is a useful
465 approach in urban flux studies. CO_2 fluxes in different landscapes measured at a single
466 site showed considerably different behaviors (Fig. 4, 6, 9). The approach previously used
467 for clarifying variations in fluxes in different landscapes involved single flux
468 measurements (Järvi et al., 2012; Kordowski and Kuttler, 2010; Hirose et al., 2015). The
469 partitioning concurrently contained the limitations in which data availability decreases
470 with partitioning. In the study area, sea-breeze circulation was dominant in the summer
471 months, resulting in a large data gap from certain wind directions (shown in section 2-3).
472 Accumulating long-term data could be useful for filling the data gap.

473   The green fraction can be useful for upscaling the annual CO_2 flux in urban areas (Fig.
474 9). The applicability of the green fraction was previously reported based on a global
475 synthesis based on eddy covariance measurements in urban areas (Nordbo et al., 2012;
476 Velasco and Roth, 2010; Ward et al., 2015); the green fraction was an index of human
477 activities (Nordbo et al., 2012). The relationship between the annual CO_2 flux and the
478 green fraction in Sakai City tended to be lower than the relationship revealed by the global
479 synthesis (Nordbo et al., 2012) (Fig. 9). This difference might indicate that the
480 relationship differs in each city or country. Other environmental variables, such as
481 biomass density (Velasco et al., 2016), might improve the scaling of CO_2 fluxes in various
482 cities. Consequently, to quantify the effects of the green fraction on CO_2 emissions in
483 various cities, further direct measurements of CO_2 fluxes at various urban sites are
484 required.

485   Upscaled annual CO_2 fluxes for the city (Fig. 10) were lower than estimated using the
486 inventory published by the government. According to the inventory, approximately 57%
487 of CO_2 emissions were associated with the industrial sector, but there was no eddy
488 covariance site in the coastal industrial region. Part of the discrepancy occurred because
489 our upscaling estimated the net flux of urban emissions and vegetative uptake, whereas
490 the inventory quantified the emissions. Hirano et al. (1996) estimated that vegetation in
491 Sakai, primarily in southern sectors, absorbed $0.87 \text{ Mt CO}_2 \text{ yr}^{-1}$ of CO_2 based on an

492 inventory-based estimate. Another reason for the discrepancy was that our estimate did

493 not include hot spot emissions, such as power plants and incineration facilities, or non-

494 CO_2 gas emissions. Oda and Maksyutov (2011) estimated that approximately half of total

495 annual CO_2 emissions were from point sources in most countries. Because our upscaled

496 CO_2 flux did not include such point sources, the CO_2 emissions from point sources could

497 be more rigorously quantified using the governmental inventory than non-point sources

498 (Oda and Maksyutov, 2011). Thus, the upscaled CO_2 flux could be useful as an additional

499 constraint, providing more information regarding CO_2 emissions from non-point sources.

500 Because our simple method potentially contained uncertainties associated with a limited

501 number of one-year eddy covariance sites, and only the consideration of the green fraction,

502 the estimates should be improved with further eddy covariance sites and additional

503 environmental variables in order to explain CO_2 fluxes.

504 The inherent limitations associated with the eddy covariance method at the urban

505 environment must be reduced and quantified in future studies. The measurement height

506 at SAC was more than ten times higher than the mean building height, although reducing

507 the height was restricted due to sporadic tall buildings. This could induce underestimates

508 of nighttime fluxes (Oke, 2006), and thus, the annual emission could be underestimated.

509 CO_2 storage within the building was not considered in our study, but must be important

510 in the late afternoon and early morning (Vogt et al., 2006). In contrast, the measurement

511 height at OPU was within the roughness sublayer (1.2 to 1.7 times the mean building and

512 tree heights), and thus fluxes were influenced by localized nearby fields (Oke, 2006).

513 Separating wind sectors using the footprint analysis may suffer uncertainties when

514 advection was trigged by wind shifts.

515

516 **5. Conclusion**

517 Based on continuous measurements using the eddy covariance method at three different

518 urban sites, the diurnal, weekly, seasonal, and spatial variabilities in the CO_2 flux were

519 evaluated in Sakai, Osaka, Japan. The urban center and university sites acted as CO_2

520 sources in all seasons. A clear weekday/holiday cycle of CO_2 emissions was observed at

521 those sites. A diurnal pattern in the urban center was correlated with those for traffic count.

522 High emissions were observed in the urban site in both the winter and summer months,

523 although the traffic did not change seasonally, suggesting that changes in gas consumption

524 influenced the seasonal variabilities. The urban park and rural area exhibited CO_2 uptake

525 during the summer months, with distinct daytime uptake. Regardless of the green fraction,

526 all landscapes considered in this study acted as an annual CO_2 source. The green fraction

527 was a useful index that explained the spatial variability in the annual CO_2 fluxes, as

528 suggested in global scale studies (Nordbo et al., 2012; Velasco and Roth, 2010). The

529 relationship based on eddy covariance data within a single city could be useful to evaluate

530 CO_2 emissions at the city scale. The network of eddy covariance measurements within a

531 city is useful for characterizing spatial and temporal variations in net CO_2 fluxes in urban

532 areas.

533

543

References

544 **References**

545 Agency for Natural Resources and Energy, 2015: *Current status of gas business*, 36pp.
546 (in Japanese)

547 Awal, M.A., Ohta, T., Matsumoto, K., Toba, T., Daikoku, K., Hattori, S., Hiyama, T., Park,
548 H., 2010. Comparing the carbon sequestration capacity of temperate deciduous forests
549 between urban and rural landscapes in central Japan. Urb. For. Urb. Greening 9, 261-
550 170.

551 Baldocchi, D., 2014. Measuring fluxes of trace gases and energy between ecosystems and
552 the atmosphere –the state and future of the eddy covariance method. Glob. Change Biol.
553 20, 3600-3609.

554 Bergeron, O., Strachan, I.B., 2011. CO_2 sources and sinks in urban and suburban areas of
555 a norther mid-latitude city. Atmos. Environ. 45, 1564-1573.

556 Canadell, J.G., Le Quéré, C., Raupach, M.R., Field, C.B., Buitenhuis, E.T., Ciais, P.,
557 Conway, T.J., Gillett, N.P., Houghton, R.A., Marland, G., 2007. Contributions to
558 accelerating atmospheric CO_2 growth from economic activities, carbon intensity, and
559 efficiency of natural sinks. Proc. Natl., Acad. Sci. 104, 18866-18870.

560 Coutts, A.M., Beringer, J., Tapper, N.J., 2007. Characteristics influencing the variability
561 of urban CO_2 fluxes in Melbourne, Australia. Atmos. Environ. 41, 51-62.

562 Crawford, B., Grimmond, C.S.B., Christen, A., 2011. Five years of carbon dioxide fluxes
563 measurements in a highly vegetated suburban area. Atmos. Environ. 45, 896-905.

564 Foken, T. Wichura, B., 1996. Tools for quality assessment of surface-based flux
565 measurements. Agric. Forest Meteorol. 78, 83-105.

566 Gioli, B., Toscano, P., Lugato, E., Matese, A., Miglietta, F., Zaldei, A., Vaccari, F.P., 2012.
567 Methane and carbon dioxide fluxes and source partitioning in urban areas: the case
568 study of Florence, Italy. Environ. Poull. 164, 125-131.

569 Gough, C.M., Vogel, C.S., Harrold, K.H., George, K., Curtis, P.S., 2007. The legacy of
570 harvest and fire on ecosystem carbon storage in a north temperate forest. Global
571 Change Biol. 13, 1935-1949.

572 Grimmond, C.S.B., King, T.S., Cropley, F.D., Nowak, D.J., Souch, C., 2002. Local-scale
573 fluxes of carbon dioxide in urban environments: methodological challenges and results

574   from Chicago. Environ. Pollut. 116, S243-S254.

575   Grimmond, C.S.B., Salmond, J.A., Oke, T.R., Offerle, B., Lemonsu, A., 2004. Flux and

576   turbulence measurements at a densely built-up site in Marseille: heat, mass (water and

577   carbon dioxide), and momentum. J. Geophys. Res. 109, doi:10.1029/2004JD004936.

578   Hirano, T., Kiyota, M., Aiga, I., 1996. Vegetation in Sakai City, Osaka, as a sink of air

579   pollutants. Bull. Univ. Osaka Pref., Ser. B 48, 55-64.

580   Hirano, T., Sugawara, H., Murayama, S., Kondo, H., 2015. Diurnal variation of CO_2 flux

581   in an urban area of Tokyo. SOLA 11, 100-103.

582   Järvi, L., Nordbo, A., Riikonen, A., Moilanen, J., Nikinmaa, E., Vesala, T., 2012. Seasonal

583   and annual variation of carbon dioxide surface fluxes in Helsinki, Finland, in 2006-

584   2010. Atmos. Chem. Phys., 12, 8475-8489.

585   Kaimal, J.C., Finnigan, J.J., 1994. Atmospheric Boundary Layer Flows, 289pp., Oxford

586   Univ. Press, New York.

587   Kanda, M., Takayanagi, Y., Yokoyama, H., Moriwaki, R., 1997. Field observations of the

588   heat balance in an urban area. J. Japan Soc. Hydrol. Water Resour. 10, 329-336.

589   Kochendorfer, J., Meyers, T.P., Frank, J., Massman, W.J., Heuer, M.W., 2012. How well

590   can we measure the vertical wind speed? Implications for fluxes of energy and mass.

591   Boundary-Layer Meteorol. 145, 383-398.

592   Kordowski, K., Kuttler, W., 2010. Carbon dioxide fluxes over an urban park area. Atmos.

593   Environ. 44, 2722-2730.

594   Kormann, R., Meixner, F.X., 2000. An analytical footprint model for non-neutral

595   stratification. Boundary-Layer Meteorol. 99, 207-224.

596   Kotthaus, S., Grimmond, C.S.B., 2012. Identification of micro-scale anthropogenic CO_2,

597   heat and moisture sources –Processing eddy covariance fluxes for a dense urban

598   environment. Atmos. Environ. 57, 301-316.

599   Latty, E.F., Canham, C.D., Marks, P.L., 2004. The effects of land-use history on soil

600   properties and nutrient dynamics in northern hardwood forests of the Adriondack

601   Mountains. Ecosystems 7, 193-207.

602   Liu, H.Z., Feng, J.W., Vesala, T., 2012. Four-year (2006-2009) eddy covariance

603   measurements of CO_2 flux over an urban area in Beijing. Atmos. Chem. Phys., 12,

604   7881-7892.

605   Lloyd, J., Taylor, J.A., 1994. On the temperature dependence of soil respiration. Funct.

606   Ecol. 8, 315-323.

607   MacDonald, R.W., Griffiths, R.F., Hall, D.J., 1998. An improved method for the

608   estimation of surface roughness of obstacle arrays. Atm. Env. 32, 1857-1864.

609   Massman, W.J., 2000. A simple method for estimating frequency response corrections for

610   eddy covariance systems. Agric. For. Meteorol. 104, 185-198.

611   Mills, G., 2007. Cities as agents of global change. Int., J. Climatol. 27, 1849-1857.

612   Moriwaki, R., Kanda, M., Nitta, H., 2006. Carbon dioxide build-up within a suburban

613   canopy layer in winter night. Atmos. Environ. 40, 1394-1407.

614   Moore, C.J., 1986. Frequency response corrections for eddy correlation systems.

615   Boundary-Layer Meteorol. 37, 17-35.

616   Nakai, T., Shimoyama, K., 2012. Ultrasonic anemometer angle of attack errors under

617   turbulent conditions. Agric. For. Meteorol. 162-163, 14-26.

618   Nimitz, E., Hargreaves, K.J., McDonald, A.G., Dorsey, J.R., Fowler, D., 2002.

619   Micrometeorological measurements of the urban heat budget and CO_2 emissions on a

620   city scale. Environ. Sci. Technol. 36, 3139-3146.

621   Nordbo, A., Järvi, L., Haapanala, S., Wood, C. R., Vesala, T., 2012. Fraction of natural

622   area as main predictor of net CO_2 emissions from cities. Goephys. Res. Lett. 39,

623   doi:10.1029/2012GL053087.

624   Oda, T., Maksyutov, S., 2011. A very high-resolution (1 km $\times$ 1 km) global fossil fuel

625   CO_2 emission inventory derived using a point source database and satellite

626   observations of nighttime lights. Atmos. Chem. Phys. 11, 543-556.

627   Oke, T.R., 2006. Initial guidance to obtain representative meteorological observations at

628   urban sites. Instruments and observing methods report No. 81, World Meteorological

629   Organization, 47pp.

630   Pawlak, W., Fortuniak, K., Siedlecki, M., 2011. Carbon dioxide flux in the center of Łódź,

631   Poland –analysis of a 2-year eddy covariance measurement data set. Int. J. Climatol.

632   31, 232-243.

633   Peters, W., Jacobson, A.R., Sweeney, C., Andrews, A.E., Conway, T.J., Masarie, K.,

634   Miller, J., Bruhwiler, L.M., Pétron, G., Hirsch, A.I., Worthy, D.E.J., van der Werf, G.R.,
635   Randerson, J.T., Wennberg, P.O., Krol, M.C., Tans, P.P., 2007. An atmospheric
636   perspective on North American carbon dioxide exchange: CarbonTracker. Proc. Natl.,
637   Acad. Sci. 104, 18925-18930.

638   Peters E.B., McFadden, J.P., 2012. Continuous measurements of net CO_2 exchange by
639   vegetation and soils in a suburban landscape. J. Geophys. Res. 117,
640   doi:10.1029/2011/JG001933.

641   Schimel, D.S., House, J.I., Hibbard, K.A., Bousquet, P., Ciais, P., Peylin, P., Braswell,
642   B.H., Apps, M.J., Baker, D., Bondeau, A., Canadell, J., Churkina, G., Cramer, W.,
643   Denning, A.S., Field, C.B., Fridlingstein, P., Goodale, C., Heimann, M., Houghton,
644   R.A., Melilo, J.M., Moore III, B., Murdiyarso, D., Noble, I., Pacala, S.W., Prentice,
645   I.C., Raupach, M.R., Rayner, P.J., Scholes, R.J., Steffen, W.L., Wirth, C., 2001. Recent
646   patterns and mechanisms of carbon exchange by terrestrial ecosystems. Nature 414,
647   169-172.

648   Stterthwite, D., 2008. Cities' contribution to global warming: notes on the allocation of
649   global greenhouse gas emission. Environ. Urbanization, 20, 539-549.

650   Ueyama, M., Hirata, R., Mano, M., Hamotani, K., Harazono, Y., Hirano, T., Miyata, A.,
651   Takagi, K., Takahashi, Y., 2012. Influences of various calculation options on heat,
652   water and carbon fluxes determined by open- and closed-path eddy covariance methods.
653   Tellus 64B, 19048, doi.org/10.3402/tellusb.v64i0.19048.

654   Ueyama, M., Iwata, H., Harazono, Y., Euskirchen, E.S., Oechel, W.C., Zona, D., 2013.
655   Growing season and spatial variations of carbon fluxes of Arctic and boreal ecosystems
656   in Alaska. Ecol. Appl. 23, 1798-1816.

657   Velasco, E., Pressley, S., Allwine, E., Westberg, H., Lamb, B., 2005. Measurements of
658   CO_2 fluxes from the Mexico City urban landscape. Atmos. Environ. 39, 7433-7446.

659   Velasco, E., Roth, M., 2010. Cities as net source of CO_2: review of atmospheric CO_2
660   exchange in urban environments measured by eddy covariance technique. Geography
661   Compass 4/9, 1238-1259.

662   Vickers, D. Mahrt, L., 1997. Quality control and flux sampling problems for tower and
663   aircraft data. J. Atmos. Oceanic Technol. 14, 512-526.

664 Vogt, R., Christen, A., Rotach, M.W., Roth, M., Satyanarayana, A.N.V., 2005. Temporal

665   dynamics of CO_2 fluxes and profiles over a Central European city. Theor. Appl.

666   Climatol. 84, 117-126.

667 Ward, H.C., Evans, J.G., Grimmond, C.S.B., 2013. Multi-season eddy covariance

668   observations of energy, water and carbon fluxes over a suburban area in Swindon, UK.

669   Atmos. Chem. Phys. 13, 4645-4666.

670 Ward, H.C., Kotthaus, S., Grimmond, C.S.B., Bjorkegren, A., Wilkinson, M., Morrison,

671   W.T.J., Evans, J.G., Morison, J.I.L., Iamarino, M. 2015. Effects of urban density on

672   carbon dioxide exchanges: observations of dense urban, suburban and woodland areas

673   of southern England. Environ. Pollut. 198, 189-200.

674 Webb, E.K., Pearman, G.I., Leuning, R., 1980. Correction of flux measurements for

675   density effects due to heat and water vapour transfer. Quart. J. Roy. Meteorol. Soc. 106,

676   85-10.

24

25

677 **Figure and table captions:**

678 Figure 1. Aerial photograph by Google Earth showing the study area, where the 80% flux

679   footprint in daytime is shown with red lines. The boundary of Sakai City is shown as a

680   yellow line.

681

682 Figure 2. Seasonal variations of (a) daily mean, maximum, and minimum air temperatures,

683   (b) daily maximum vapor pressure deficit (VPD) and daily total rainfall. Temperatures

684   and VPD were measured at 111 m above the ground at the SAC site and rainfall was

685   measured at the OPU site, during 2015. Temperatures and VPD are shown as a 7-day

686   running mean.

687

688 Figure 3. Relative wind frequency distributions at the three sites during the study period

689   in 2015. Data are binned in 45° classes.

690

691 Figure 4. Mean diurnal variations of (a) CO_2 fluxes and (b) traffic count at two highway

692   exits within the flux footprint of SAC west. The diurnal patterns were created every

693   consecutive three months in 2015. Because measurements at IZM began in February

694   2015, diurnal variations for IZM during the period from January to March were

695   calculated based on data from February and March in 2015 and January in 2016.

696

697 Figure 5. Relationships between the CO_2 flux and solar radiation measured at (a) the urban

698   park in IZM, (b) the rural area in IZM, and (c) OPU sites during the period from July

699   to September of 2015.

700

701 Figure 6. Seasonal variations of the daily mean (a) CO_2 fluxes and (b) the gross

702   photosynthetic flux in 2015, shown as 7-day running means.

703

704 Figure 7. Relationship between the daily mean air temperature and the daily mean CO_2

705   flux; CO_2 flux data were binned at 3°C intervals.

706

707 Figure 8. Averaged daily CO_2 flux for each day of the week in 2015 for (a) SAC west and

708 (b) OPU; fluxes for holidays were averaged separately. Vertical lines represent standard

709 deviation.

710

711 Figure 9. Relationship between the annual CO_2 flux (F_{CO2}) and the green fraction (f_G).

712 The solid line represents a regression based on our flux data for Sakai, and the dashed

713 line represents a relationship based on a global synthesis (Nordbo et al., 2012).

714

715 Figure 10. Spatial distributions of (a) the green fraction and (b) the upscaled net CO_2 flux

716 in Sakai City. The green fraction was calculated at a 500-m spatial resolution based on

717 an inventory of green spaces.

718

719 Figure A1. Relative wind frequency distributions at the three sites during the study period

720 in 2015 for each season. Data are binned in 45° classes.

721

722 Figure A2. Mean diurnal variations of CO_2 fluxes at (a) SAC west, (b) SAC east, (c) OPU,

723 (d) the urban park in IZM, and (e) the rural area in IZM during the period from April

724 to September. The date are shown as the 1.5-hours running means. Sunny days were

725 defined as days when the precipitation was less than 5 mm d^{-1}, and the daily sum of

726 solar radiation was greater than 80% of that expected from solar geometry.

727

728 Figure A3. Seasonal variations in monthly gas consumption rates at Osaka Prefecture

729 University for 2015. The data are shown for 16 buildings in the west-sector of the

730 university, where flux measurements were conducted, and for four buildings located

731 within the flux footprint.

732

733 Table 1. Land cover fraction within d the daytime flux footprint. Landcover classification

734 was conducted using the Digital Map 5000 for the Kinki region in 2008 by the

735 Geospatial Information Authority of Japan, and the green space fraction was based on

736 a green census by the government of Sakai City. Because the land cover classification

737 and green space are different data sources, the sum of each fraction often exceeds 100%.

738 The daytime flux footprint was calculated using the analytical footprint model

739 (Kormann and Meixner, 2000), and median values in 2015 were classified for sixteen

740 directions (Fig. 1).

741

742 Table 2. Annual CO_2 fluxes from the eddy covariance measurements and the upscaled

743 city-scale flux.

Table 1. Land cover fraction within d the daytime flux footprint. Landcover classification was conducted using the Digital Map 5000 for the Kinki region in 2008 by the Geospatial Information Authority of Japan, and the green space fraction was based on a green census by the government of Sakai City. Because the land cover classification and green space are different data sources, the sum of each fraction often exceeds 100%. The daytime flux footprint was calculated using the analytical footprint model (Kormann and Meixner, 2000), and median values in 2015 were classified for sixteen direction (Fig. 1).

	SAC west	SAC east	OPU	IZM park	IZM rural
	%	%	%	%	%
Residence	27	9	9	1	15
Commercial, industrial, and public offic	34	38	69	6	15
Road	27	29	10	3	6
Green space	14	27	44	72	62

Table 2.   Annual CO_2 fluxes from the eddy covariance measurements and the upscaled city-scale flux.

Site	CO_2 flux $g\ C\ m^{-2}\ yr^{-1}$
SAC west	4948
SAC east	3134
OPU	1270
IZM park	802
IZM rural	495
Upscale	3325

Figure 1
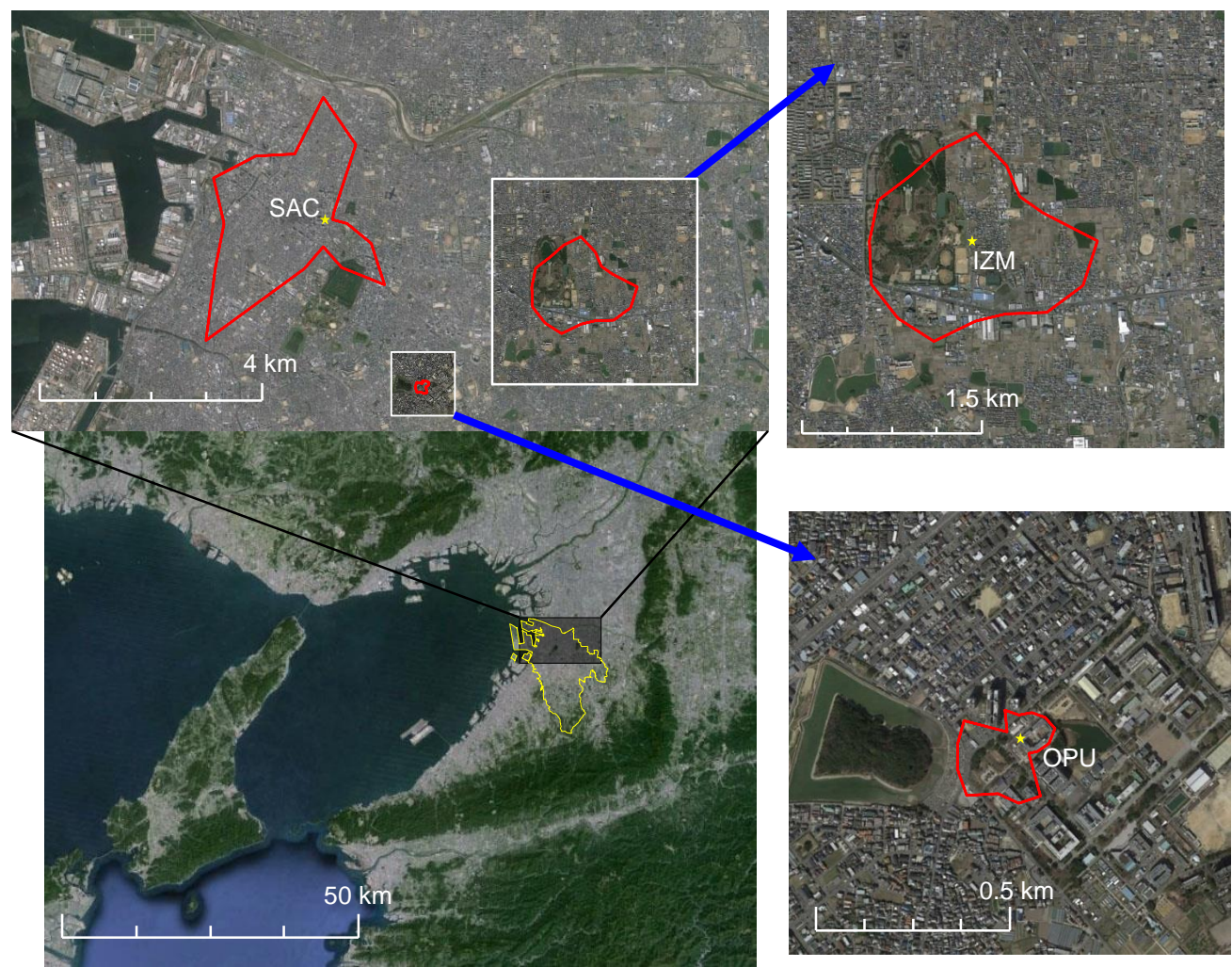
Fig. 1.   Aerial photograph by Google Earth showing the study area, where the 80% flux footprint in daytime is shown with red lines. The boundary of Sakai City is shown as a yellow line.

Figure 2
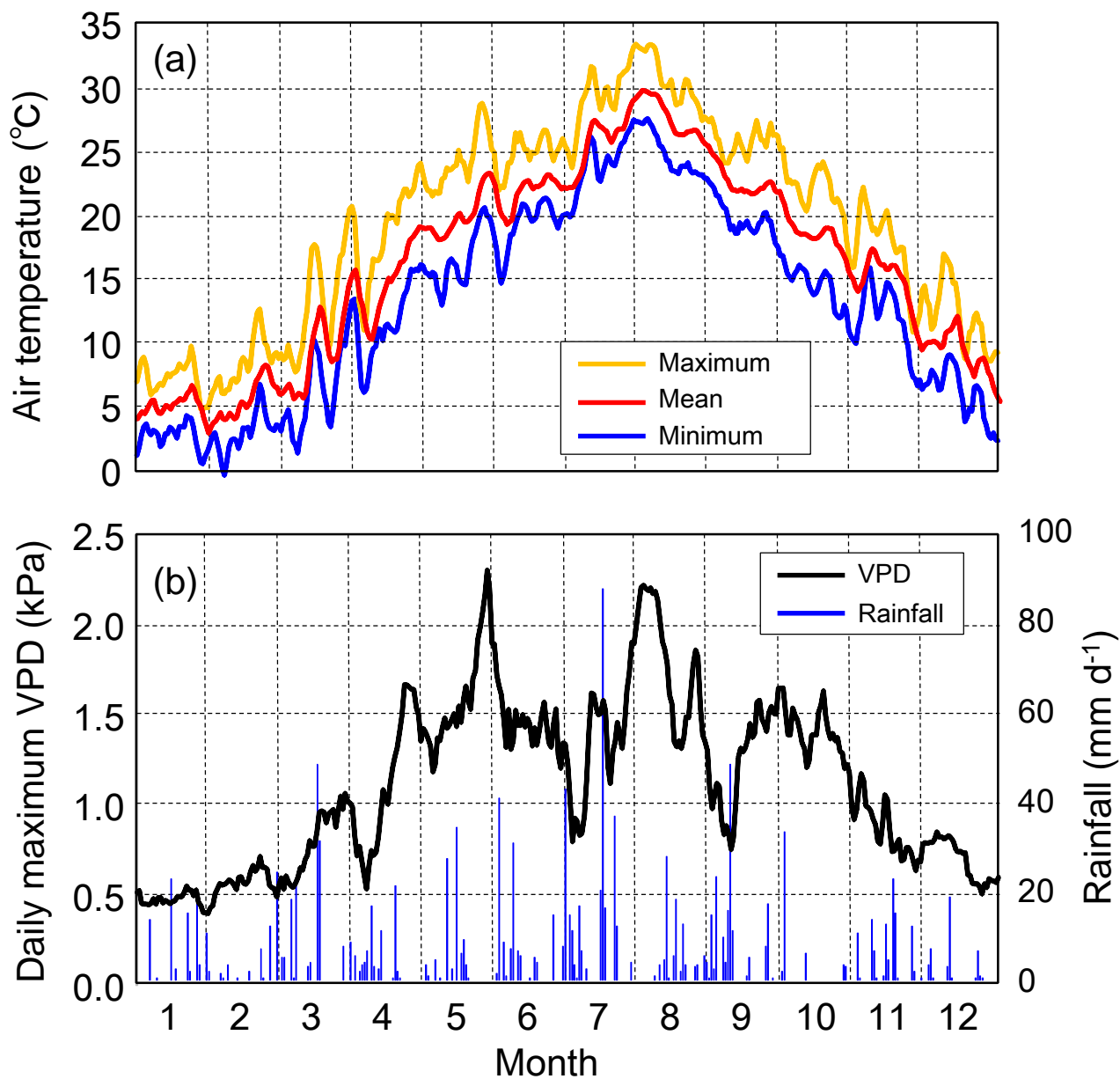
Fig. 2.   Seasonal variations of (a) daily mean, maximum, and minimum air temperatures, (b) daily maximum vapor pressure deficit (VPD) and daily total rainfall. Temperatures and VPD were measured at 111 m above the ground at the SAC site and rainfall was measured at the OPU site, during 2015. Temperatures and VPD are shown as a 7-day running mean.

Figure 3

(a) SAC (b) OPU (c) IZM

Legend:
> 2 – 3 m s⁻¹   > 3 - 5 m s⁻¹   > 5 - 7 m s⁻¹   > 7 - 9 m s⁻¹   > 9 - 11 m s⁻¹
> 11 - 13 m s⁻¹   > 13 - 15 m s⁻¹   > 15 - 17 m s⁻¹   > 17 m s⁻¹
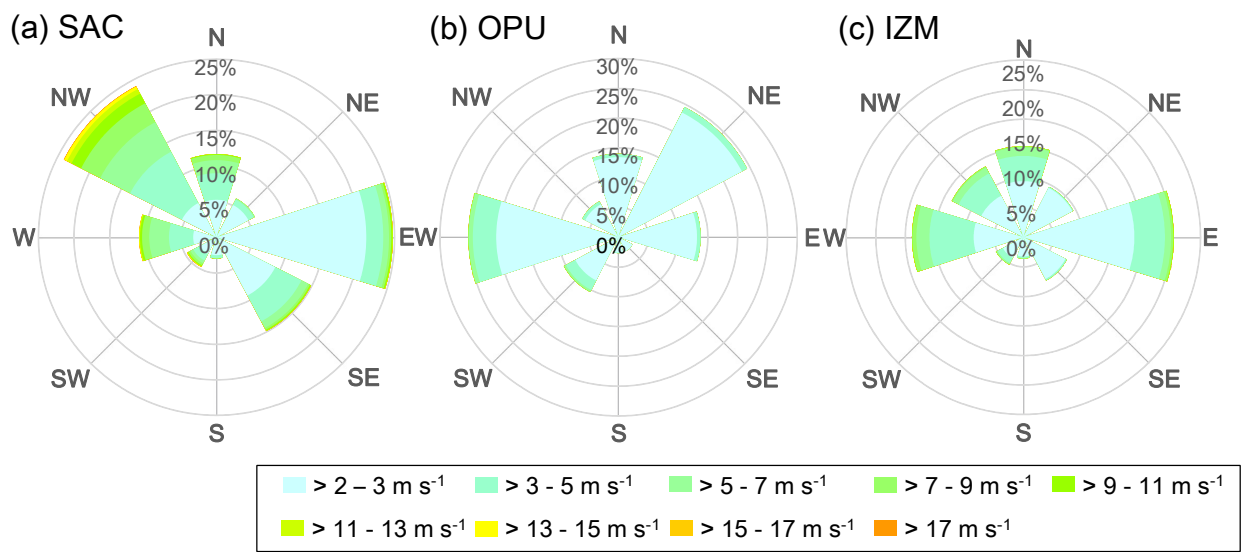
Fig. 3.   Relative wind frequency distributions at the three sites during the study period in 2015. Data are binned in 45° classes.

Figure 4
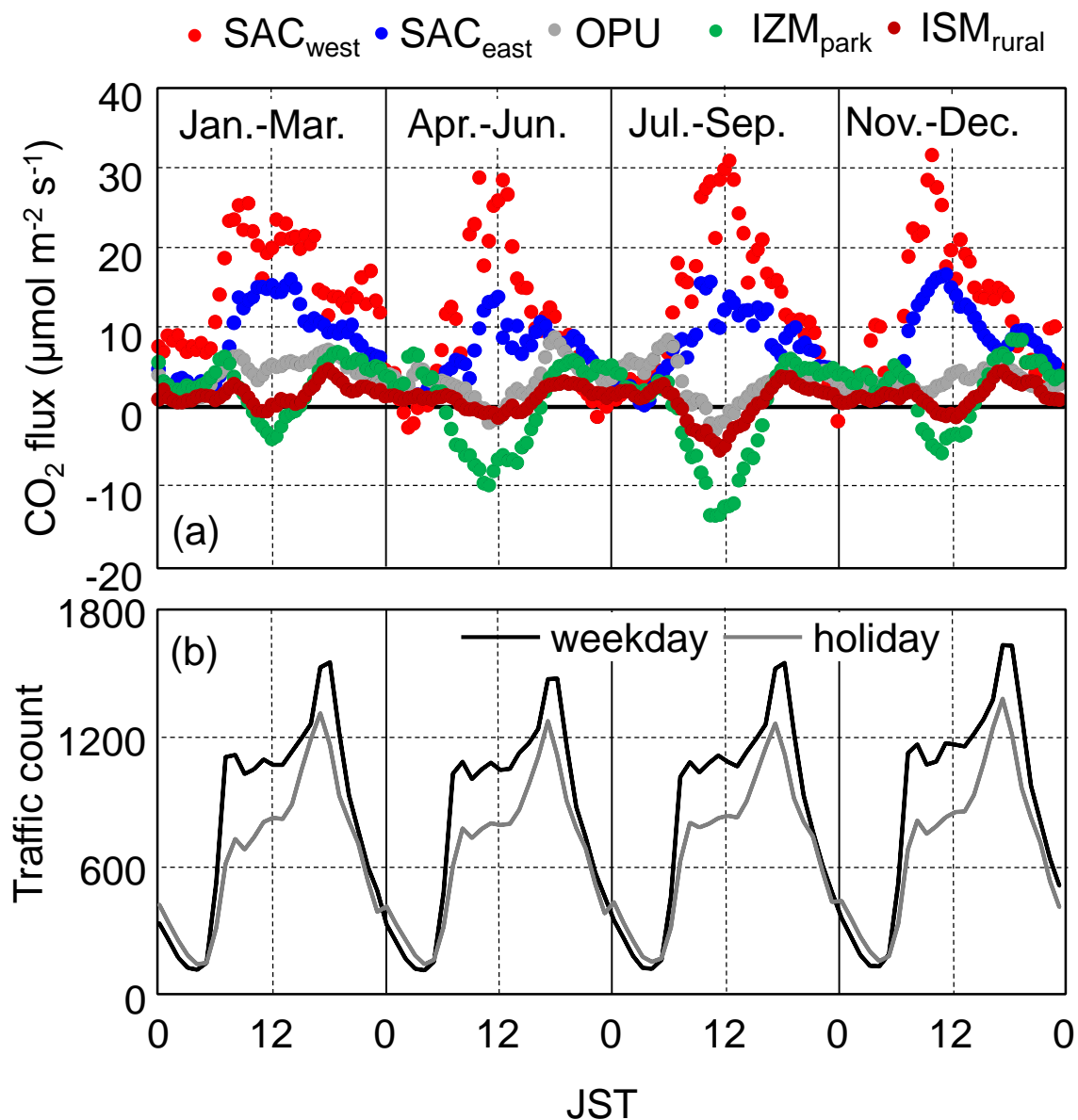
Fig. 4.   Mean diurnal variations of (a) CO_2 fluxes and (b) traffic count at two highway exits within the flux footprint of SAC west. The diurnal patterns were created every consecutive three months in 2015. Because measurements at IZM began in February 2015, diurnal variations for IZM during the period from January to March were calculated based on data from February and March in 2015 and January in 2016.

Figure 5
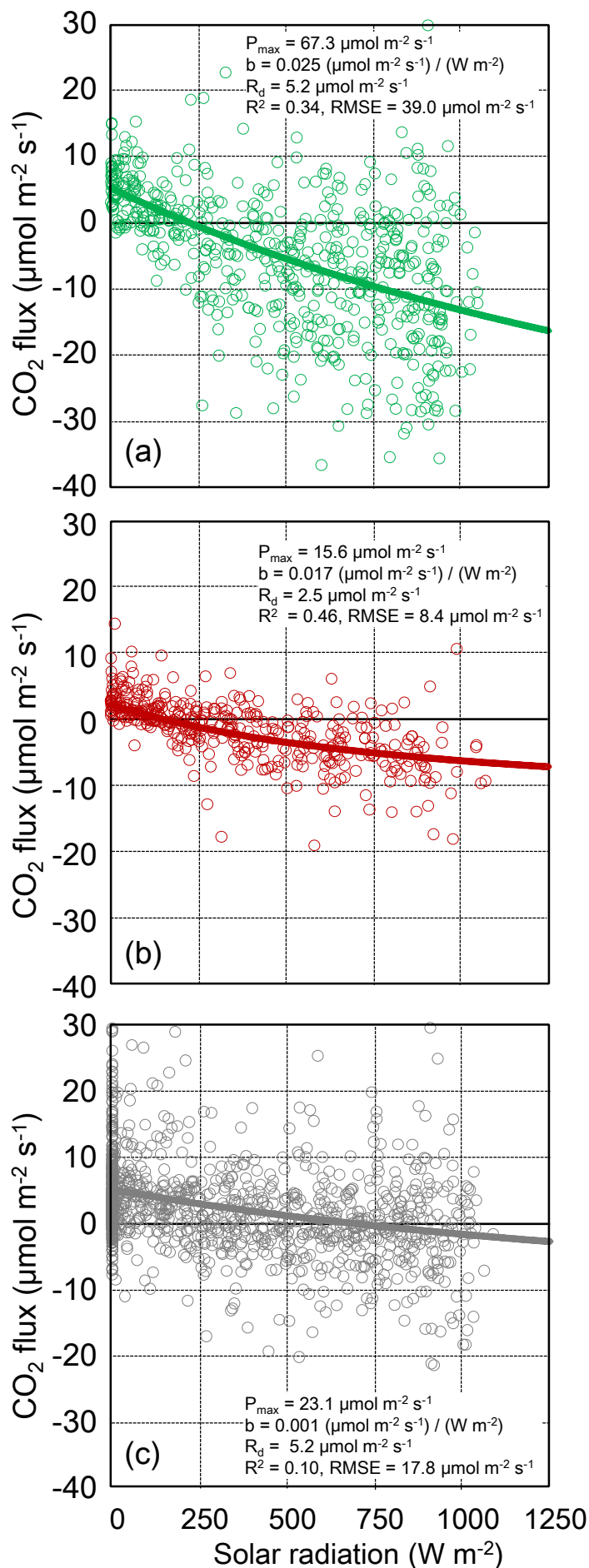
Fig. 5.

Relationships between the CO_2 flux and solar radiation measured at (a) the urban park in IZM, (b) the rural area in IZM, and (c) OPU sites during the period from July to September of 2015.

Figure 6
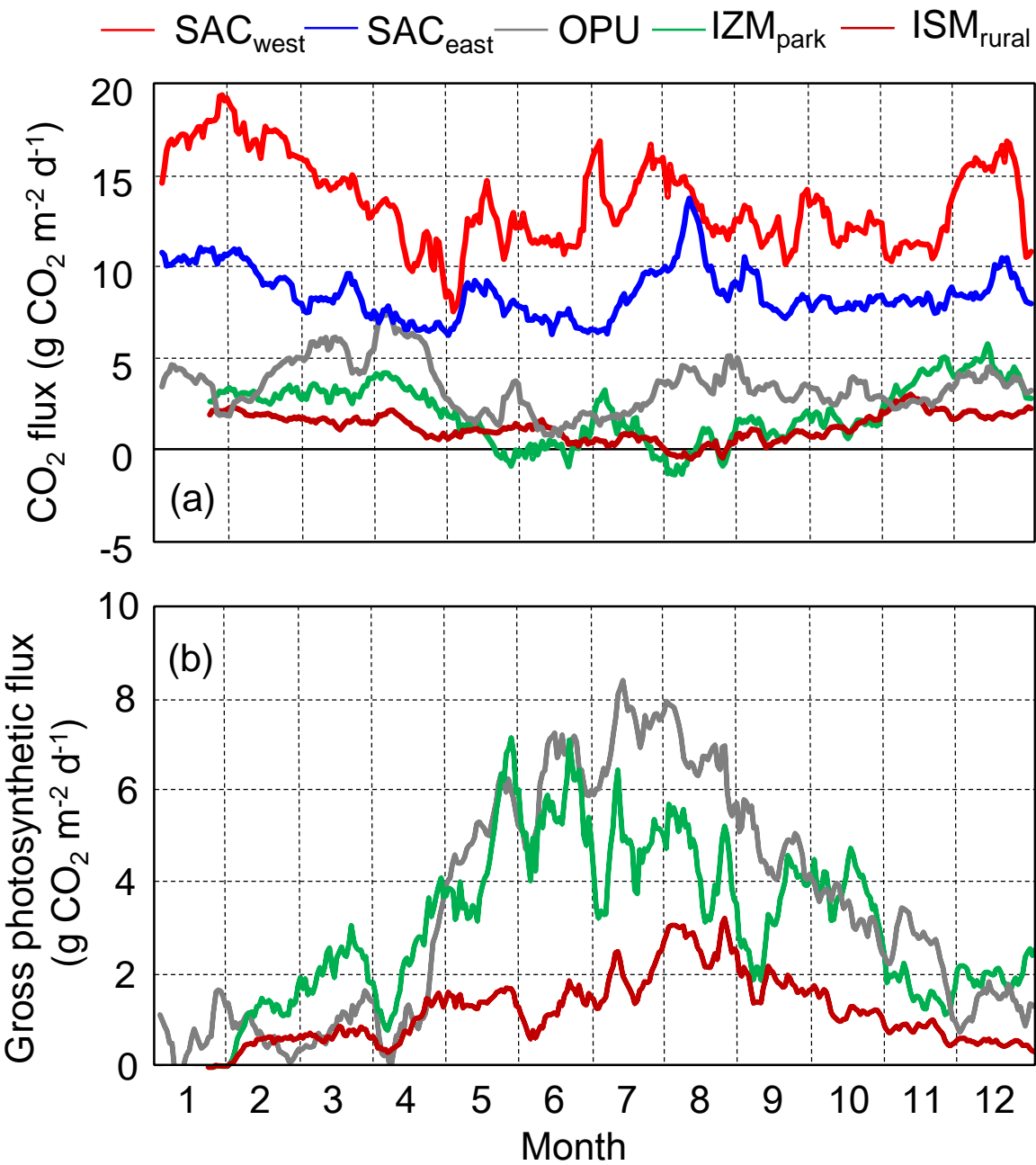
Fig. 6.   Seasonal variations of the daily mean (a) CO_2 fluxes and (b) the gross photosynthetic flux in 2015, shown as 7-day running means.

Figure 7
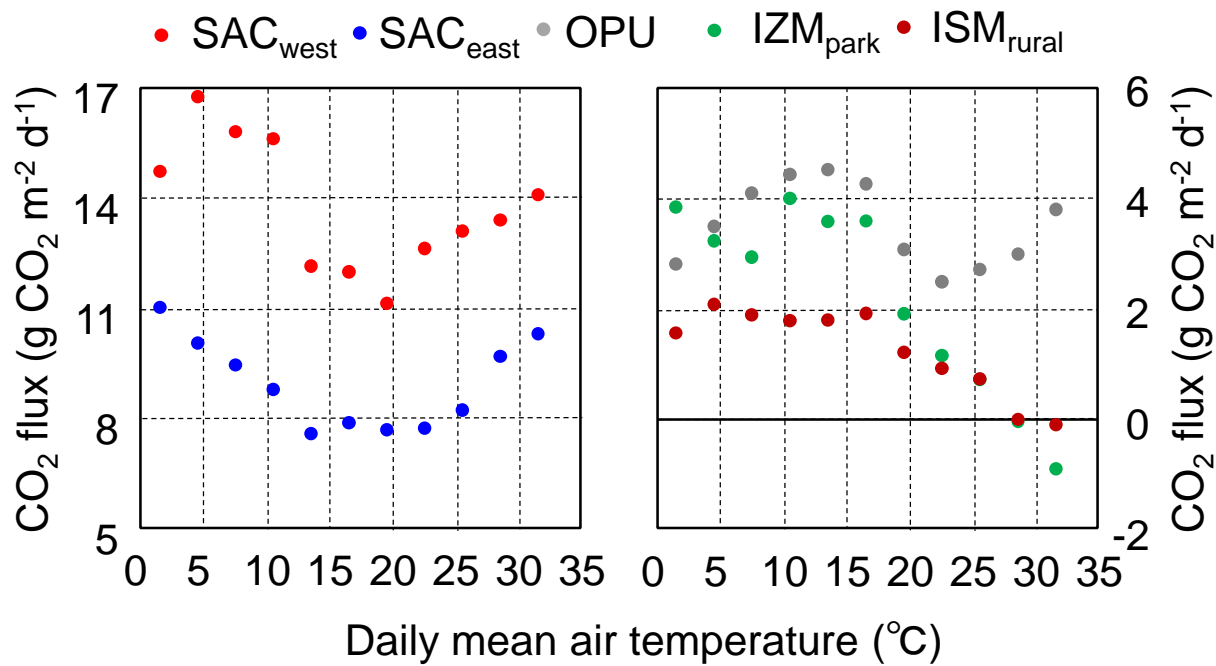
Fig. 7.   Relationship between the daily mean air temperature and the daily mean CO_2 flux; CO_2 flux data were binned at 3° C intervals.

Figure 8
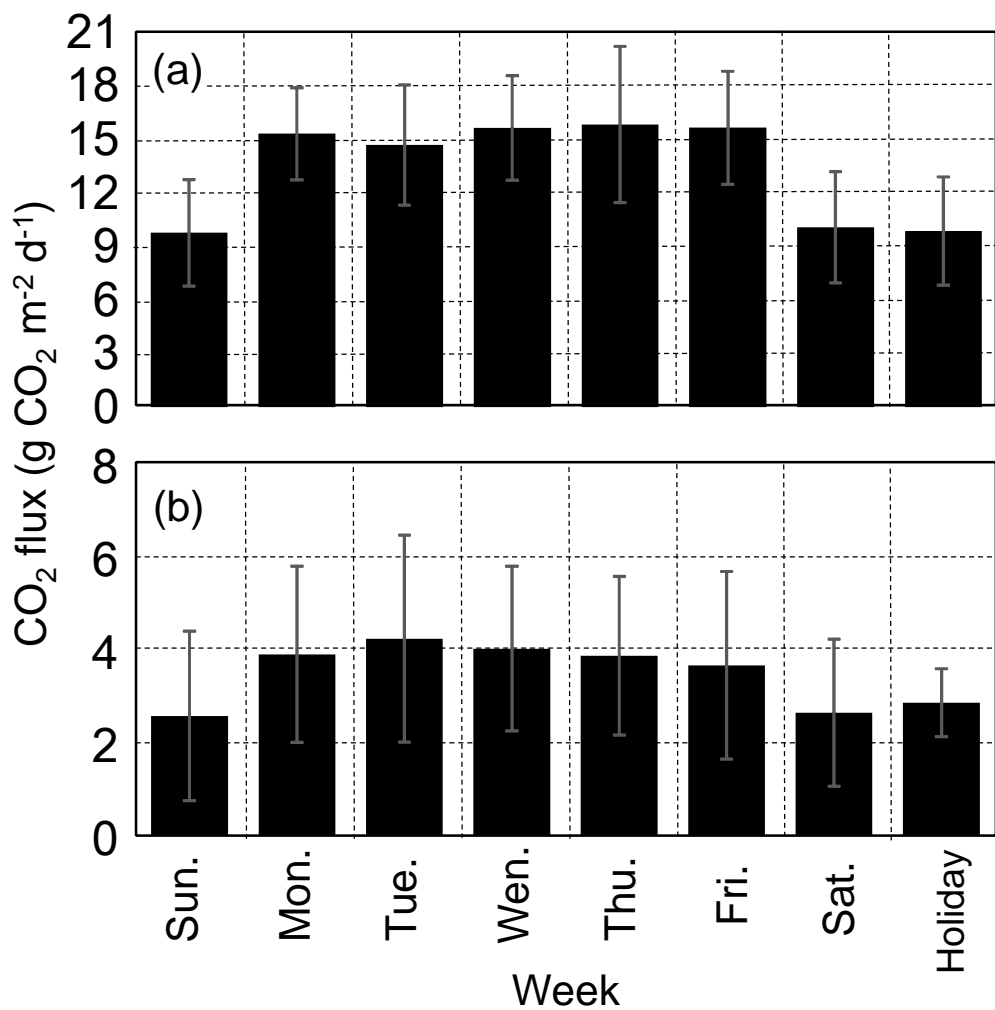
Fig. 8.   Averaged daily CO_2 flux for each day of the week in 2015 for (a) SAC west and (b) OPU; fluxes for holidays were averaged separately. Vertical lines represent standard deviation.

Figure 9
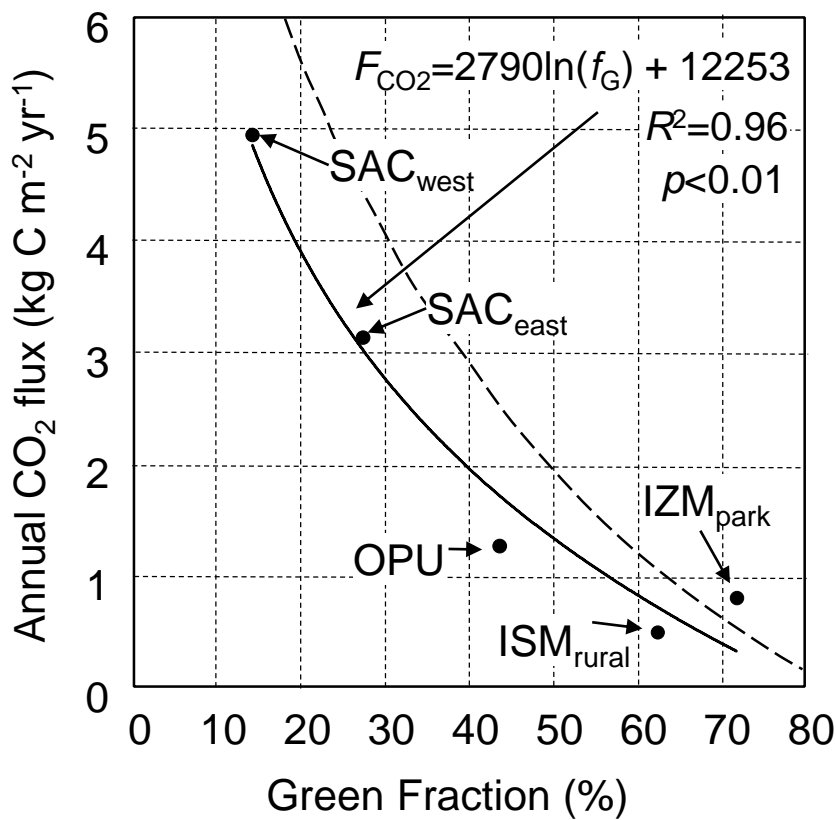
Fig. 9.　Relationship between the annual CO_2 flux (F_{CO2}) and the green fraction (f_G). The solid line represents a regression based on our flux data for Sakai, and the dashed line represents a relationship based on a global synthesis (Nordbo et al., 2012).

Figure 10
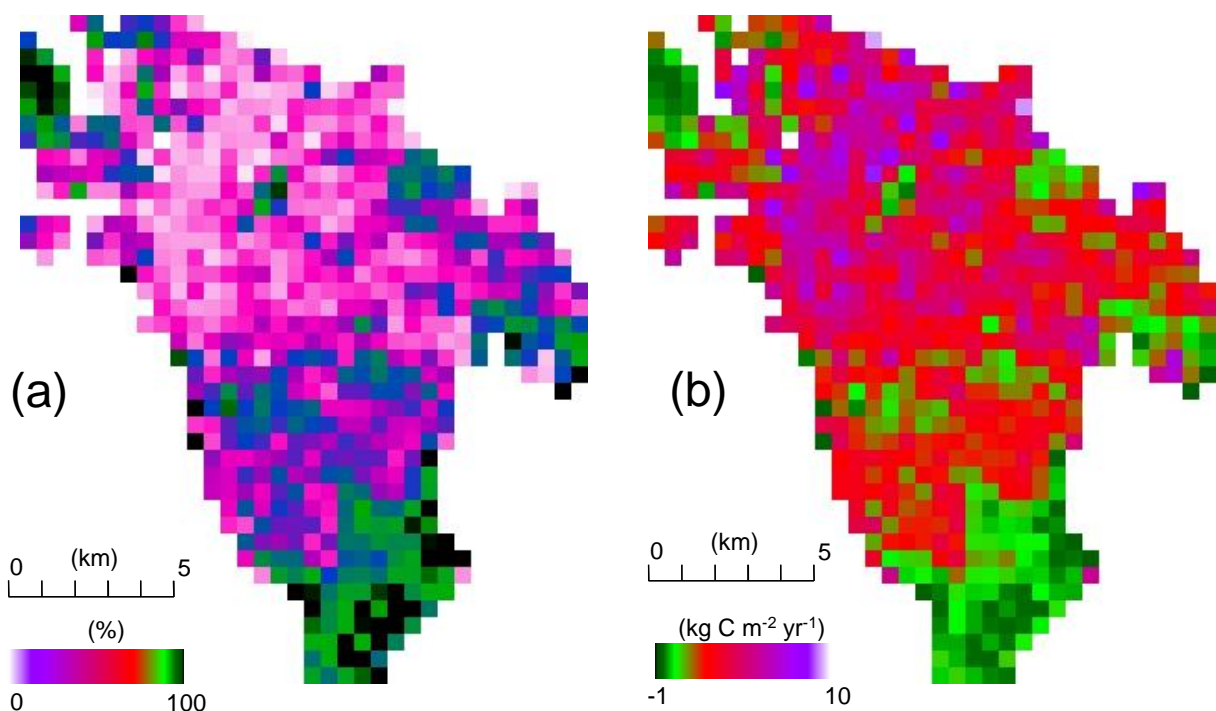
Fig. 10. Spatial distributions of (a) the green fraction and (b) the upscaled net CO_2 flux in Sakai City. The green fraction was calculated at a 500-m spatial resolution based on an inventory of green spaces.
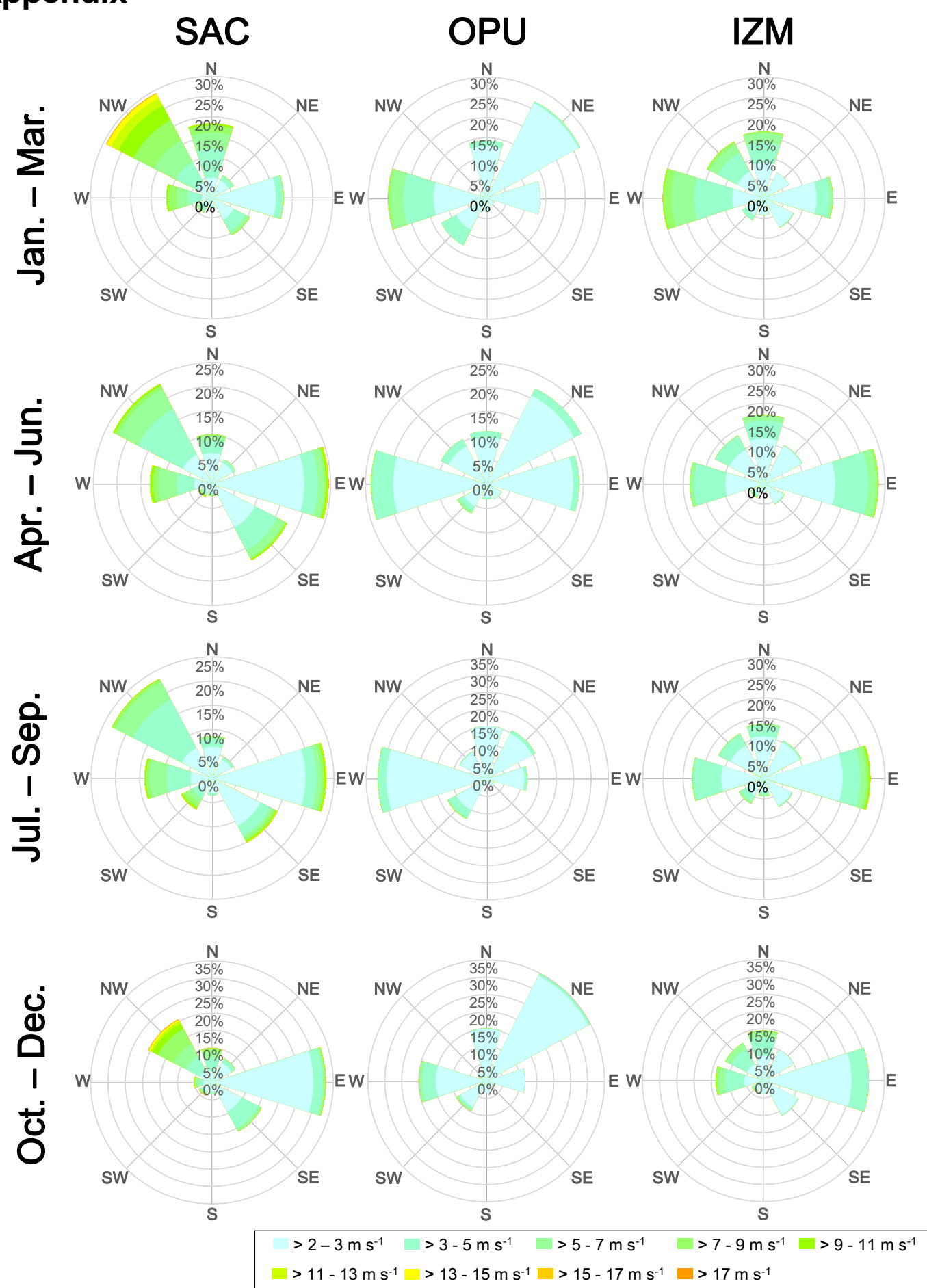
Appendix

Fig. A1. Relative wind frequency distributions at the three sites during the study period in 2015 for each season. Data are binned in 45° classes.
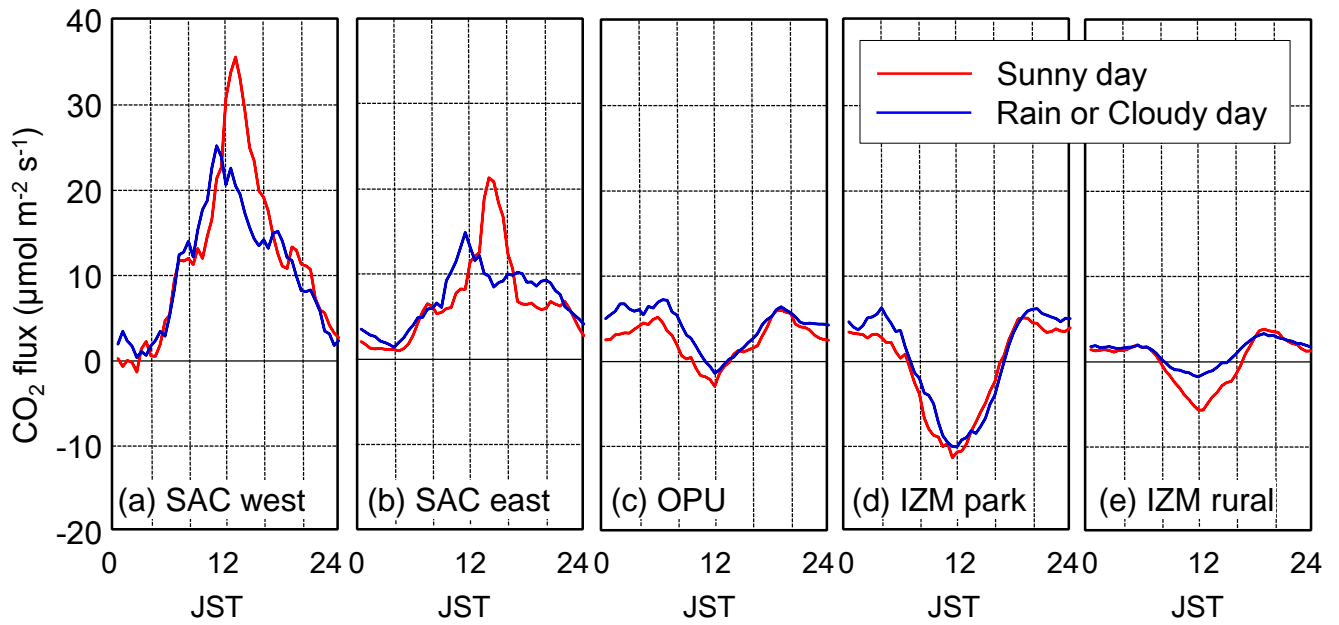
Appendix

Fig. A2.   Mean diurnal variations of CO_2 fluxes at (a) SAC west, (b) SAC east, (c) OPU, (d) the urban park in IZM, and (e) the rural area in IZM during the period from April to September. The date are shown as the 1.5-hours running means. Sunny days were defined as days when the precipitation was less than 5 mm d^{-1}, and the daily sum of solar radiation was greater than 80% of that expected from solar geometry.
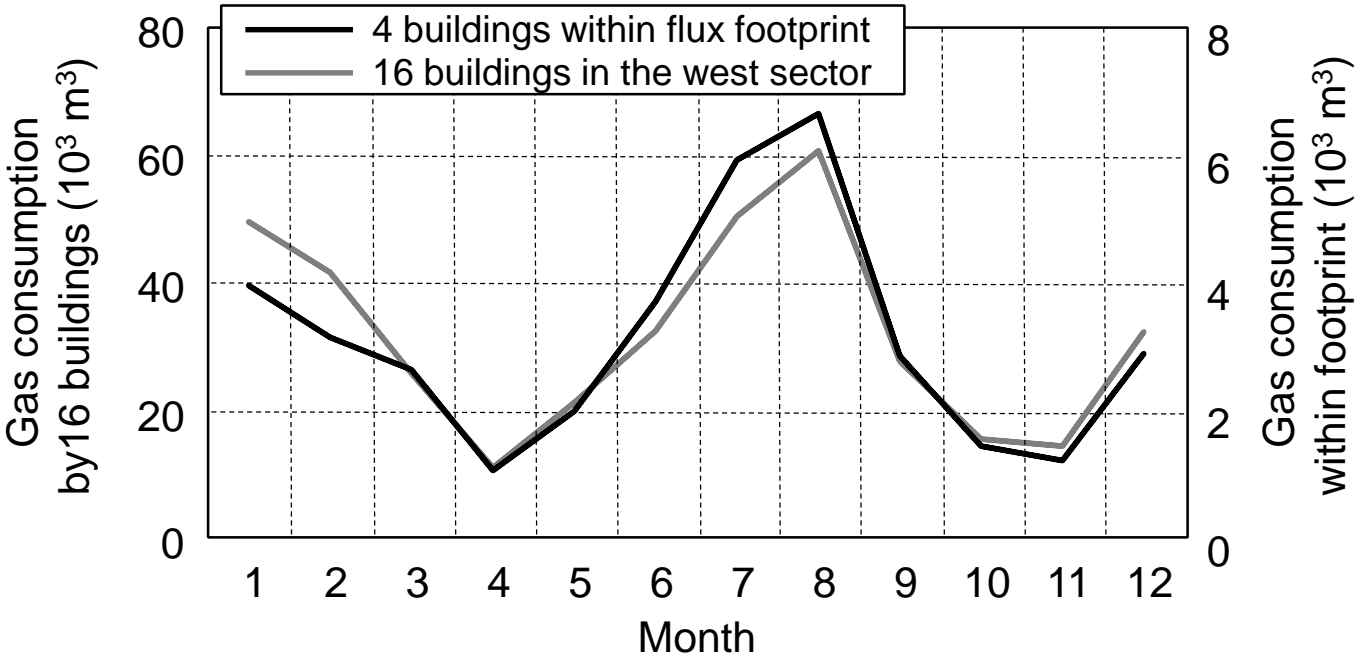
Appendix

Fig. A3. Seasonal variations in monthly gas consumption rates at Osaka Prefecture University for 2015. The data are shown for 16 buildings in the west-sector of the university, where flux measurements were conducted, and for four buildings located within the flux footprint.